# *Oxygen Adsorption on Au–Ni(111) Surface Alloys*



**Citation:** Leon, Christopher C., Jae-Gook Lee, and S. T. Ceyer. "Oxygen Adsorption on Au–Ni(111) Surface Alloys." The Journal of Physical Chemistry C 118, no. 50 (December 18, 2014): 29043–29057.

**As Published:** http://dx.doi.org/10.1021/jp503758t

**Publisher:** American Chemical Society (ACS)

**Persistent URL:** http://hdl.handle.net/1721.1/97695

**Version:** Author's final manuscript: final author's manuscript post peer review, without publisher's formatting or copy editing

# Oxygen Adsorption on Au-Ni(111) Surface Alloys

Christopher C. Leon, Jae-Gook Lee[+], S. T. Ceyer[*]

*Department of Chemistry, Massachusetts Institute of Technology, 77 Massachusetts Avenue, Cambridge, Massachusetts, USA, 02139-4307*

**ABSTRACT**: Molecular $O_2$ dissociates upon interaction with a Ni(111) surface as the spatial and energetic overlap between the Ni 3d electrons and the $O_2$ antibonding orbitals is quite favorable. On a Au-Ni(111) surface alloy where the extent of this overlap is greatly reduced, exposure to $O_2$ results in adsorption of molecular $O_2$ characterized by three peroxo- or superoxo-like vibrational bands centered at 743, 856, and 957 $cm^{-1}$ as observed by high resolution electron energy loss spectroscopy. These bands correspond to the stretch vibrational mode of $O_2$ at respective adsorption sites of type pseudo-3-fold fcc/hcp, degenerate-pseudo-2-fold fcc/hcp and bridge, and pseudo-3-fold bridge. These unusual chemical environments are brought about by surface alloying, rather than the presence of Au clusters on Ni, and are further stabilized by a dramatic reconstruction of the top two surface layers, as explained with an idealized surface alloy model in conjunction with electronic structure considerations. The ability to adjust the relative populations of the different oxygen cohorts by varying the Au content suggests the utility of surface alloy motifs for engineering applications.

**Keywords**

Surface science, high resolution electron energy loss spectroscopy, gold catalysis, surface reconstruction, d-band model.

## I. INTRODUCTION

Unlike the Group 10 elements Pd[1,2,3] and Pt,[4,5,6,7,8] Ni has not been observed to physisorb nor chemisorb molecular $O_2$. Instead, molecular $O_2$ dissociates readily upon interaction with a Ni(111) surface, even when the crystal temperature is as low as 8 K.[9] Hence, the upper limit of the barrier to dissociative chemisorption is approximately 0.016 kcal/mol. This almost-barrierless dissociation is due to the energetically favorable overlap between the Ni 3d electrons and the $O_2$ antibonding orbitals[10] because of the higher energy of the Ni 3d band relative to the Pd 4d band and Pt 5d band.

As part of a low temperature CO oxidation study, molecular $O_2$ has been shown to be stabilized on a Au-Ni(111) surface alloy that is formed by deposition of Au onto a Ni(111) surface.[11,12] The Au atoms displace Ni atoms, forming a hexagonally closed packed alloy. The Au atoms intersperse randomly among the top layer Ni atoms while keeping the two dimensional structure of the original Ni surface.[13] In addition, the formation of the Au-Ni alloy lowers the energy of the Ni 3d band center smoothly from Ni- to more Au-like with increasing Au coverage as shown via photoelectron spectroscopy.[14] This fact results in less favorable energetic overlap with the $O_2$ antibonding orbitals, thereby quenching $O_2$ dissociation. Molecular $O_2$ adsorbed at 77 K on Au-Ni alloy surfaces is characterized by O-O vibrational bands spanning 740–990 $cm^{-1}$ as obtained via high resolution electron energy loss spectroscopy (HREELS). Very similar frequencies from analogous measurements on Pd, Pt, and Ag[15,16,17] are evidence for peroxo- ($O_2^{2-}$) and superoxo-like ($O_2^{1-}$) species as these internal $O_2$ stretches are much lower in frequency from gas phase $O_2$, 1580 $cm^{-1}$. These lower $O_2$ stretch mode frequencies are a result of charge transfer from the metal to the $O_2$ antibonding orbitals, the extent of which is too low for barrierless dissociative chemisorption of $O_2$ as on Ni.

This manuscript presents vibrational spectra of molecular $O_2$ adsorbed on Au-Ni(111) alloys held at 80 K up to a Au coverage of 0.73 ML (0.8 ML is the saturation coverage) and analyzes changes in both $O_2$ adsorption (from dissociative to molecular to non-adsorption) and $O_2$ adsorption sites on the Au-Ni(111) surface with increasing Au coverage. We establish that alloy formation between Au and Ni rather than the presence of Au clusters on Ni is necessary for molecular $O_2$ adsorption at 80 K. To facilitate understanding of the experimental results, an idealized model of the surface alloy valid at all Au coverages is described prior to presenting the data. Next, we apply Nørskov's d-band model[18] to qualitatively describe electronic structure changes to Ni upon alloying with Au and its effect on $O_2$ adsorption. With both of these models, we can reconcile the results of prior scanning tunneling microscopy (STM) studies with our new observations of molecular $O_2$ adsorption on Au-Ni(111) obtained via HREELS.

## II. BACKGROUND – SURFACE MORPHOLOGY

As the incorporation of Au atoms into the Ni(111) surface is an activated, kinetically hindered process, the morphology of the surface alloy is strongly dependent on surface treatment. Our description of these surfaces is largely based on Nielsen's STM studies.[19] Below 0.3 ML Au, Au atoms directly swap for Ni atoms at surface lattice sites without disturbing the supporting layer. These swaps occur at random positions for all Au coverages. All of these alloy surfaces are compressively strained because the Au(111) lattice constant is nearly 16% larger than that of Ni(111). The surface atoms and their supporting lattice atoms do not relax to relieve this strain below 0.3 ML Au.

An extremely complex phase transition occurs just beyond 0.3 ML Au (or possibly 0.4 ML Au[20]) as accommodating extra Au atoms exceeds the maximum compressive surface strain possible without lattice reconstruction. At this coverage, the top layer lattice constant abruptly

increases while the supporting layer lattice constant remains the same. The top two layers now behave as two separate layers of atoms with different lattice constants. To reduce the interfacial strain between these two layers, some atoms are expelled from the supporting layer (and are assumed to be incorporated into the top layer) while others concurrently shift within the supporting layer. The concerted motion of these subsurface Ni atoms is poorly understood. This strain is perturbatively affected by the layer of atoms immediately below it, as these third layer atoms determine whether surface atoms are coordinated to face-centered-cubic (fcc)- or hexagonal-closed-packed (hcp)-like 3-fold hollow sites. The ratio of fcc- to hcp-like 3-fold hollow sites in the top layer drops from that of unity on a Ni(111) surface when the reconstruction takes place.

To understand this phase transition, first consider a fictitious monolayer of Au(111) physisorbed on Ni(111) (or equivalently, 0.8 ML where a ML is defined relative to the unit cell of Ni(111)) and weakly interacting with it. Figure 1 shows a top view of this system with Au and Ni atoms respectively drawn as large and small transparent circles. A moiré pattern is seen due to the lattice mismatch. The Au overlayer unit cell has a p(9×9) structure and its area is 81 times larger than the Ni(111) primitive unit cell. Its sides, shown as bold lines, are drawn so its corners align with points of 3-fold rotational symmetry. Though this choice of unit cell is not intuitive, it centers the atoms with the lowest coordination numbers in the unit cell's lower half.

The thin lines mark domain walls that split the top Au layer into triangular and hexagonal regions where Au atoms coordinate differently to the underlying Ni atoms. They are nearly 3-fold (fcc or hcp) coordinated in the former, but nearly 2-fold (bridge) and 1-fold (atop) coordinated in the latter. Atoms with intermediate coordination numbers are also present on the surface. These domains show that without surface reconstruction, a large proportion of surface

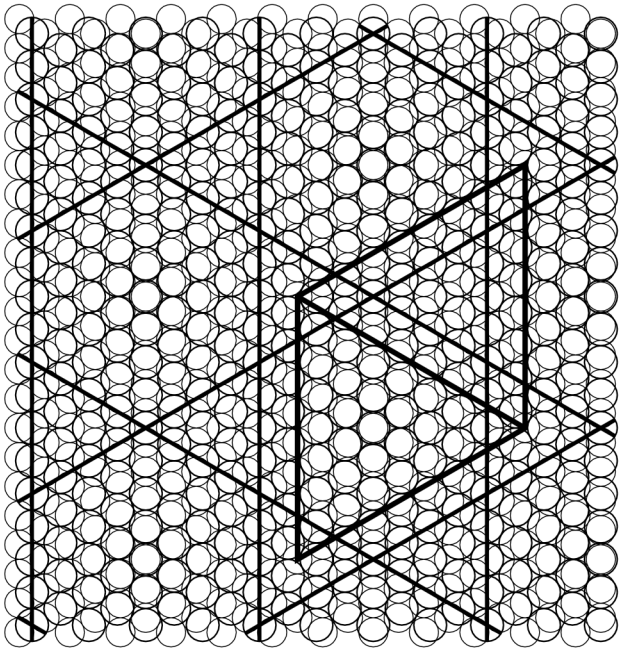

Figure 1. Triangular and hexagonal domains in an idealized p(9×9) Au(111) on Ni(111) with thin line domain walls. In the former, the Au atoms are nearly 3-fold (hcp/fcc) coordinated with the underlying Ni atoms. In the latter, the Au atoms are pseudo- 2-fold (bridge) and 1-fold (atop) coordinated with the underlying Ni atoms. Top and bottom halves of a sample unit cell are drawn with thicker lines.

atoms would rest almost directly over Ni atoms, which is an energetically unfavorable configuration. Those under-coordinated atoms are so strained that a novel subsurface reconstruction one atomic layer below the surface occurs. This reconstruction is driven by minimizing the total surface energy. This minimum occurs when the top layer atoms are maximally coordinated by resting near 3-fold hollow sites formed from the atoms in the supporting layer. With the top layer atoms fixed, the interfacial strain is reduced by forming a stacking fault in the supporting Ni layer whereby some supporting Ni atoms originally in fcc sites shift to hcp ones. The result is a subsurface, triangular misfit dislocation loop that sharply demarcates this reconstructed region located inside the hexagonal domain of every unit cell. This reconstruction raises the coordination number of many top layer atoms. Those atoms that

were minimally coordinated in a pseudo-1-fold manner to the supporting layer become maximally pseudo-3-fold coordinated.

We choose a fictitious 0.53 ML Au surface with a p(13×13) unit cell to illustrate these transformations more clearly. As in Figure 1, we choose to position the unit cells in Figure 2 so that their lower halves are all centered on the reconstructed region. This Au coverage is coincidentally near the middle of the 0.3–0.8 ML Au interval where reconstruction occurs. The unit cell periodicity $p$ is a function of the normalized gold coverage $\theta = \theta_{Au}/0.8$ given by $p = 1+a_{Ni}/[\theta(a_{Au}-a_{Ni})]$ with $a_{Ni} = 2.489$ Å being the Ni atom diameter and $a_{Au} = 2.8$ Å being the empirically measured length between Au atom centers within a Au island adsorbed on Ni(111).[19] The subsurface Ni atoms in the p(13×13) unit cell that form an idealized triangular misfit dislocation loop are shaded in Figure 2a. The chain of atoms to be removed are shaded more darkly. Its length is about half the moiré periodicity and is also nearly the side length of the resulting loop. Removal of this chain of Ni atoms allows those atoms remaining in the triangular region to shift left by the distance between the center of a 3-fold hollow and any of its three nearest atop sites. The result is shown in Figure 2b with the reference center unmoved from that in Figure 2a. The chain in Figure 2a can also be removed from any of three symmetrically equivalent orientations to obtain the same configuration shown in Figure 2b. In Figures 2c and 2d, the centers of the overlayer atoms are shown in relation to both non-reconstructed and reconstructed Ni lattices, respectively. Without reconstruction, the centers of 28 surface atoms are directly, or very nearly on top of supporting Ni atoms (Figure 2c). No atop coordinated surface atoms exist after the reconstruction (Figure 2d).

As seen in Figure 2d, 18 top layer atoms in each unit cell sink into the shaded loop and enclose 10 atoms in its interior. The center of this entire group of 28 atoms is on average,

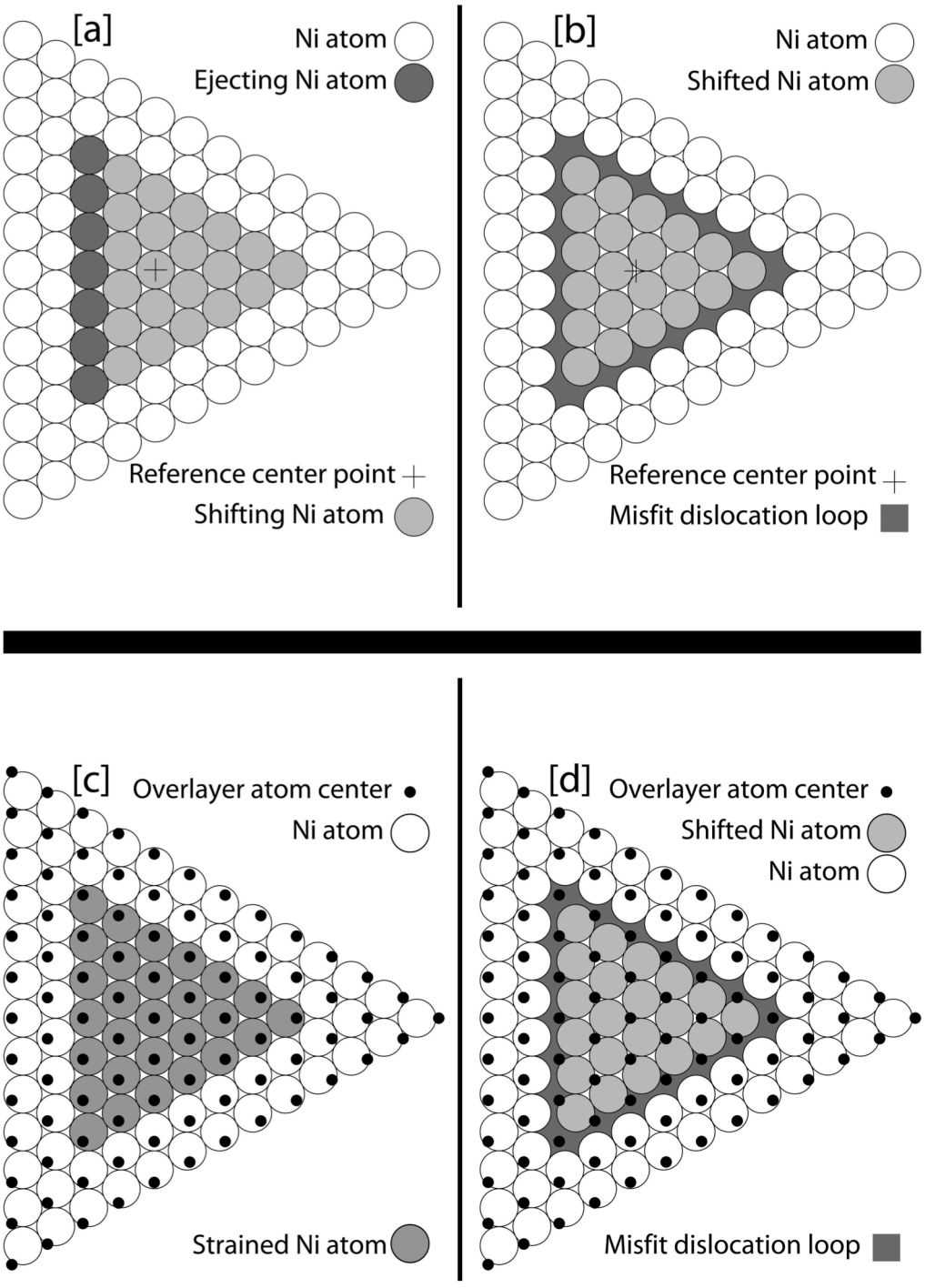


Figure 2. Subsurface Ni atoms and their movement within a half of a p(13×13) Au-Ni(111) unit cell before [a] and after reconstruction [b]. The coordination number of the top layer atoms [c] increases dramatically [d] as a result.

coincident with the center of the non-reconstructed hexagonal domain. This new triangular

domain is different from those other triangular domains shown in Figure 1 that are manifestly present on the surface due to the moiré patterned atomic positions. Since STM images show a large contrast between the reconstructed triangular enclosure and its interior, earlier descriptions[21] of the reconstructed triangular region adopted a convention of counting the number of atoms fully inside the dislocation loop as indicative of its size. Although a practical choice, we think the more natural variable to use is the edge length of the triangular loop (which is 7 in the case of Figures 2 and 3), as it matches the number of subsurface Ni atoms removed and is nearly half the moiré periodicity.

In Figure 3, the 0.53 ML Au unit cell is shown with identically shaded substrate atoms indicating distinct surface electronic environments. Subsurface layer atoms are respectively either pseudo- 3-fold or 2-fold coordinating based on the atoms' proximity to a triangular or hexagonal domain. Chemically similar surface atoms are thought to be resting on top of matching shaded regions. However, atoms at and near the loop experience very strong electronic structure perturbations. Fewer subsurface atoms are near the loop corners, so surface atoms at those locations embed proportionally deeper into the bulk compared to those along the loop lengths. Arguably, all sunken atoms (which are those directly over the dislocation loop in Figure 3) have higher coordination numbers to the underlying Ni atoms compared to any other surface atom. The 15 top-layer atoms in the loop edge are pseudo-4-fold coordinated to the underlying Ni atoms, and the 3 atoms at the corners are pseudo-5-fold coordinated. The atom fraction affected by this loop later explains the relative ratios of adsorbed molecular oxygen species on the alloy surface.

With our surface model, we can quantitatively reproduce Nielsen's description of representative misfit dislocation loops as a function of Au coverage.[19] This correspondence is

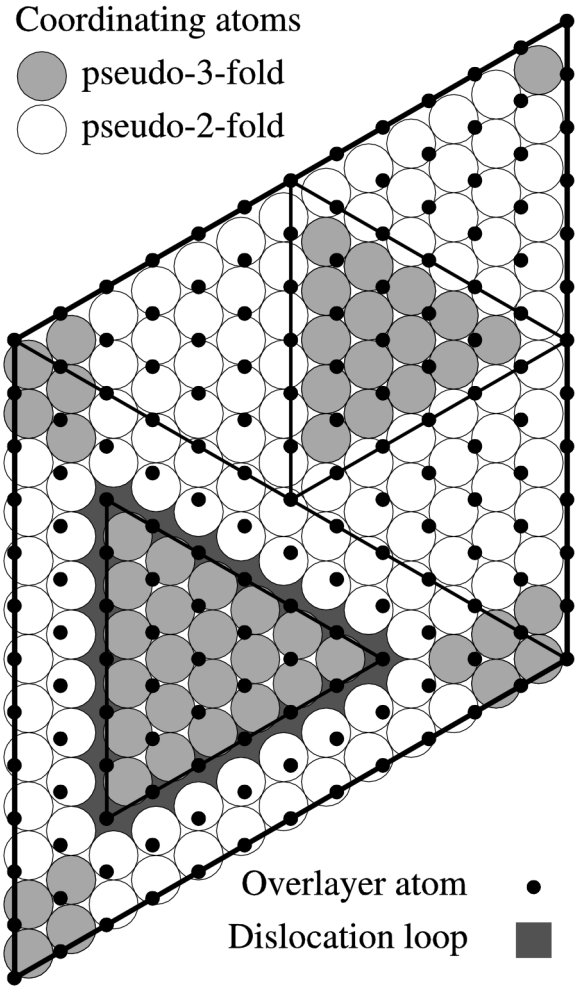


Figure 3. 0.53 ML Au model unit cell.

possible because the domain sizes in the unit cell are dependent on the underlying moiré pattern periodicity, and this periodicity in turn is dependent on the average size of all atoms that constitute the very top layer. Those prior STM measurements established that the effective lattice constant of the entire surface layer is the average of the lattice constant of a pure Au layer and a pure Ni layer weighted by the Au coverage. Our model complements this result by further clarifying how the atoms within the unit cell are spatially related to each other before and after the reconstruction, and emphasizes the existence of distinct domains and electronic environments within the unit cell in addition to those within the reconstructed region. These domains of

pseudo-2- and 3-fold coordinated surface atoms are well defined so long as the Au atoms are dispersed with sufficient randomness. This randomness is important as otherwise an effective model unit cell cannot be constructed.

Based on this unit cell model and our experimental data, we will later propose that while two non-degenerate cohorts of molecular $O_2$ co-adsorb onto these pseudo-3-fold coordinated regions, two degenerate cohorts of molecular $O_2$ (appearing as one cohort) adsorb onto pseudo-2-fold coordinated regions. These regions are assigned as the binding sites of three intense molecular $O_2$ bands seen in HREELS. This model relies on knowing that the electronic structure of the topmost layer is distinctly heterogeneous within the length scale of half the moiré periodicity. Although the topmost layer consists of Au and Ni atoms thoroughly intermixed, large regions of surface atoms rest atop distinct electronic environments due to the relative positions of surface atoms with respect to the supporting layer. Experimental preparation of these alloy surfaces is discussed in the next section.

## III. EXPERIMENTAL

**A. Procedure.** Experiments are conducted in a molecular beam ultra-high vacuum apparatus[22] with a base pressure less than $5\times10^{-11}$ Torr. A Ni(111) single crystal, oriented to within 0.2°, can be cooled to 80 K, heated radiatively to 450 K by a W filament mounted behind the crystal, or heated to 1300 K by electron bombardment via biasing the crystal relative to the filament. The crystal is cleaned via repeated cycles of $Ar^+$ ion sputtering followed by annealing to between 1000–1300 K. Surface cleanliness is verified by the absence of contaminants as detected by Auger electron spectroscopy (AES) and HREELS. Two additional stringent tests of surface homogeneity and HREELS consistency are performed by translating the crystal relative to the electron beam, and verifying that Auger intensities or vibrational loss features obtained in each

position are coincident.

Gold (Alfa Aesar, Premion, 99.999%) is vapor-deposited at an adjustable rate between 0.01–0.60 ML Au/min onto the Ni(111) crystal held at 450 K and then annealed at 773 K for 10 minutes. This procedure renders the alloy surface nearly atomically smooth at all Au coverages. The Au coverage is first estimated during deposition using a quartz crystal microbalance[23] contained within the Au source and then accurately determined after deposition via curve fitting of Au and Ni Auger intensities. Uniformity of the Au dose is verified by measuring the Au coverage at 19–22 distinct positions on the crystal. The Au coverage uniformity is deemed acceptable only if the dispersion, defined as the ratio of the standard deviation to the average of all measured Au coverages on a single prepared surface, is less than 4%. Results presented here were measured on surfaces with dispersions of 3.8% or lower. The non-uniformity of Au coverage is the dominant contribution to surface alloy heterogeneity. Additional sources of imprecision include the statistical error in the peak-to-peak measurements that results in a standard deviation of $5.5\times10^{-3}$ ML Au error in each Au coverage measurement. The published error in sensitivity factors also contributes an additional relative error on the order of $4\times10^{-5}$ to the final assigned Au coverage.

All $O_2$ exposures are effected using a 10% mixture of scientific grade $O_2$ (MG Scientific) in pure Ar (Spectra Gases) supplied as a beam. The chamber geometry is such that the entire crystal surface, held at 80 K, is exposed to the beam. The estimated $O_2$ exposure of 4–5 L is chosen to saturate the vibrational loss features seen between 700–1200 $cm^{-1}$ near 0.46 ML Au.[12]

HREEL spectra are measured using a spectrometer described previously.[24] The elastically scattered beam of electrons has a full width at half maximum (FWHM) of less than 60 $cm^{-1}$ and an average peak intensity of 44 kHz with a range of 5.7–170 kHz. Spectral acquisition time is

approximately one hour using a channel width of 8 $cm^{-1}$. All spectra are recorded with an impact energy of 5.5 eV at the specular angle incident at 60˚ to the normal, and normalized to 500 kHz total count rate in the fitted elastically scattered loss feature. All HREEL intensities are absolute and normalized in an identical manner. We assume based on near edge x-ray absorption fine structure measurements[25] of Ag and Pt, that molecular $O_2$ on Au-Ni(111) also adsorbs with its principal axis parallel to the surface. Charge transfer to the surface fluctuating along with the internal stretch vibrational motion results in a changing dipole moment with a perpendicular component to the surface.[26] Therefore, the stretch vibrational mode is dipole active and inelastically scatters electrons which are detected optimally in the specular direction.

**B. Coverage Calibrations via Auger Measurements.** Gold and oxygen coverages are determined using a semi-empirical analysis of Auger electron spectra acquired in derivative mode using 2 kV electrons incident at the normal angle. Associated intensities and linewidths are estimated with the peak-to-peak method and assumed to have derivative Gaussian profiles. Spectrometer drifts are compensated by averaging over multiple, separate scans.

**1. Gold coverage calibration via Auger spectroscopy**. The Au coverage is defined as the mole fraction of Au atoms accommodated within the top surface layer, which is the ratio between the Au (74 eV) Auger transition intensity and the sum of the Au (74 eV) plus Ni (64 eV) Auger transition intensities. All transition intensities are divided by their absolute cross section.[27] The intensities are determined from fits of two derivative Gaussians centered near 64 and 74 eV to the experimental data. However, this method underestimates the Au coverage because the experimental Ni intensity originates from Ni atoms both below and at the surface.

To estimate the intensity solely from the Ni surface atoms, we treat the Auger signal as originating from four independent sources: surface Ni and Au atoms, and bulk Ni atoms

occluded by those two sets of surface atoms. Next, we assume that the signal from surface atoms and their occluded counterparts is a fixed ratio for all Au coverages. The Ni intensity arising from subsurface Ni atoms occluded by surface Au atoms can now be estimated by rescaling the measured Au signal with this ratio. Subtracting this estimate from the total measured Ni intensity yields the Ni intensity originating from Ni atoms without the influence of Au. A final rescaling of this quantity with the same ratio gives the desired intensity from just the Ni surface atoms. This ratio of surface to bulk intensity is determined from the Ni Auger intensity measured at $\theta = 55^\circ$ from the normal angle of a Ni(111) crystal, using the electron mean free path at 2 keV and 64 eV obtained from the universal curve. This ratio is defined as $I_{surface} / I_{bulk} = e^{3L/2} - e^{L/2}$ with $L = (\lambda_{in}^{-1}+\lambda_{out}^{-1}\sec\theta)(\alpha/\sqrt{3})$ which results from electron screening in successive [111] layers of nickel[23] while assuming the topmost Ni atoms screen to a depth of half the lattice plane spacing. The Ni lattice constant $\alpha$ is taken to be 3.52 Å. The mean free paths $\lambda_{in}$ and $\lambda_{out}$ in nanometers are calculated according to $\lambda = 143(E+W)^{-2} + 0.054(E+W)^{1/2}$ with the incoming and outgoing electron energy $E$ set to 2000 eV and 64 eV respectively. The Ni(111) surface work function $W$ is taken to be 5.35 eV.[28] Using these parameters, we find that the relative intensity from the bulk is 0.519 when the signal from surface atoms is normalized to unity.

As this method for Au coverage calibration uses known absolute ratios of Au and Ni Auger transition intensities, it is considered superior to our previous method that required a comparison to previous results from another laboratory[29] and that yielded Au coverages about a factor of two smaller than the present values. Our present method of absolute Au coverage determination also accounts for the relative sizes of Au and Ni atoms. That is, the minimum Au coverage required to block oxygen adsorption completely is observed to be 0.8 ML Au via HREELS. This

coverage is equivalent to a hexagonally close packed layer of larger Au atoms adsorbed on 1 ML of smaller Ni atoms on Ni(111). This coincidence supports our absolute Au coverage assignments as very little to no oxygen adsorption is expected at 80 K on a completely Au covered surface with no Ni sites exposed.

As our results were obtained with a Ni crystal exposed to Au for several years, a residual 0.14–0.16 ML Au is detectable via AES even when the Ni crystal is not exposed to Au. This Au arises from the resurfacing[30] of a very small quantity of Au dissolved in Ni as the solubility of Au in Ni is not zero[29] (even though the two metals do not form a bulk alloy). Our results for the Ni surface without exposure to Au are identical to those gathered when the Ni surface had never been exposed to Au or had been exposed to Au for lesser periods of time. Since this residual Au appears to minimally perturb the Ni surface, the composition of the first few layers beneath the surface is assumed to be purely Ni.

**2. Oxygen coverage calibration via Auger spectroscopy**. Absolute oxygen coverage assignments are based on a conversion factor of 0.8168 $ML^{-1}$, which is the experimentally determined ratio of the O (510 eV) to Ni (849 eV) Auger peak-to-peak transition intensities at 0.25 ML O atom coverage. This p(2×2) reference surface is prepared by exposing Ni(111) at 300 K to 1.5 L $O_2$ in small increments while monitoring for an abrupt change in the ratio of O to Ni Auger intensity per unit $O_2$ exposure. This change signals a large drop in dissociative chemisorption probability[31] for Ni(111) oxidation beyond 0.25 ML. The same conversion factor is used on all Au-Ni surfaces to determine absolute oxygen coverage. These coverage assignments agree with a semi-empirical method (involving absolute cross sections[27] in place of conversion factors) to within 0.02 ML when averaged over all experimentally measured Au coverages.

## IV. RESULTS

Molecular oxygen dissociates on Ni(111) at 80 K, resulting in adsorbed O atoms. HREELS reveals a single dominant loss feature centered at 600 $cm^{-1}$ with a less intense shoulder near 480 $cm^{-1}$, as shown in Figure 4a. The former arises from atomic oxygen adsorbed in 3-fold hollow sites[32] and is the symmetric Ni-O stretch while the latter is attributed to oxygen within bulk-like nickel oxide environments. Additionally, a weak overtone of the surface oxygen stretch is detectable at 1120 $cm^{-1}$. The longitudinal $S_2$ surface phonon[33] is also observable near 260 $cm^{-1}$.

Deposition of 0.55 ML Au onto Ni(111) held at 80 K is presumed to result in Au clusters supported on Ni(111).[34] Subsequent exposure to $O_2$ results in the formation of adsorbed O

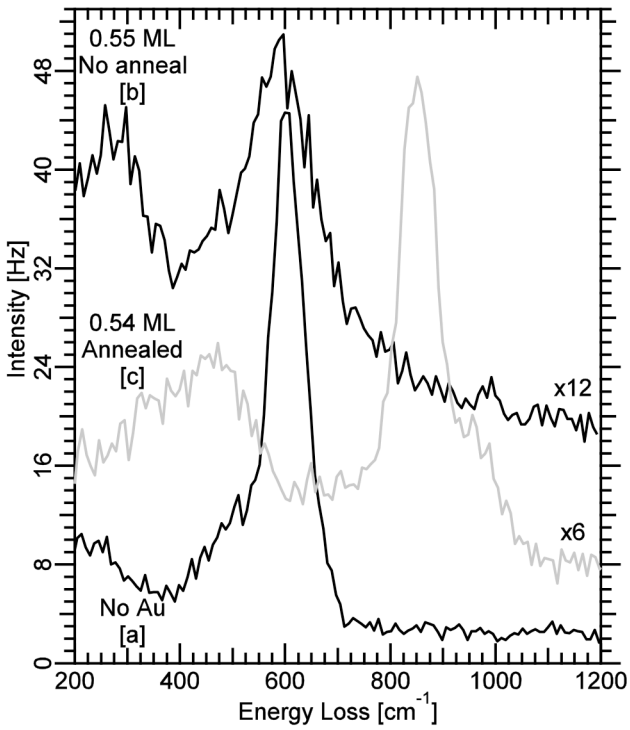


Figure 4. Annealing Au into Ni(111) is key for molecular $O_2$ adsorption. Shown are HREELS spectra measured after exposure to $O_2$ of Ni(111) with no Au deposited [a], and 0.54–0.55 ML Au deposited on Ni without annealing [b] and with annealing [c].

(Figure 4b) with the loss feature near 600 $cm^{-1}$ significantly broadened and reduced in intensity, while surface phonon intensity appears noticeably enhanced. The broadening is presumed to signal O atom adsorption on Ni atoms that are affected by neighboring Au atoms. This control experiment shows that Au deposited in this manner is insufficient to significantly modify the high probability of $O_2$ dissociative adsorption on Ni(111) even as Au atoms block those sites.

However, if Au deposition is followed by annealing at 773 K, Au atoms incorporate into the topmost layer of the Ni(111) crystal and form a stable Au-Ni surface alloy.[35] Subsequent exposure to $O_2$ results in a profound change in vibrational loss features. The light trace in Figure 4c shows distinctly enhanced loss features associated with the internal vibrational stretch of molecularly adsorbed $O_2$ between 700–1100 $cm^{-1}$ along with a concomitant reduction of loss features associated with atomically adsorbed O. The presence of loss features associated with molecular $O_2$ adsorbed on the surface alloy prepared by annealing is in stark contrast to their absence on the non-annealed surface. Only the combination of Au deposition and subsequent annealing causes new vibrational features to appear in the vicinity of 855 $cm^{-1}$ after exposure to $O_2$. Also, the very small feature near 980 $cm^{-1}$ in the dark trace representing the non-annealed surface might be molecular $O_2$ stabilized near Au clusters. These observations establish the utility of $O_2$ as a probe molecule for understanding the unusual chemical environments present on appropriately prepared Au-Ni surfaces.

Surfaces prepared as above are part of a large family of Au-Ni surface alloys.[29] Incorporating Au atoms into the Ni(111) surface through annealing dramatically changes the surface electronic structure. Rather than pure Au clusters on Ni(111), it is the incorporation and dispersion of Au atoms within the Ni surface that enables molecular $O_2$ adsorption. Our desire to understand the origin of this molecular $O_2$ stabilization prompted the collection of a

comprehensive set of vibrational spectra of $O_2$ on Au-Ni surface alloys as a function of Au coverage.

Figure 5 presents HREEL spectra measured after exposure of Au-Ni surface alloys at 80 K to 4–5 ML of $O_2$. The spectra are arranged with Au coverage increasing from bottom to top, from no Au deposition to just shy of complete passivation of the Ni surface at 0.8 ML Au. Our point of discussion begins with the spectrum at the bottom of Figure 5.

In the case of no Au exposure, $O_2$ dissociatively adsorbs and 0.33 ML O atoms are deposited under our experimental conditions. As the Au coverage is raised, the Ni-O stretch at 600 $cm^{-1}$ shifts lower in frequency and its intensity drops at a rate inversely proportional to the 12th power of the Au coverage (not shown) until it is unobservable between 0.32–0.37 ML Au. This rate suggests that a single Au atom affects both its nearest Ni neighbors and slightly beyond. The quenched 600 $cm^{-1}$ feature also reflects the drop in $O_2$ dissociative adsorption probability caused by the Ni 3d band center lowering in energy with increasing Au coverage. The intensity change of the surface phonon near 270 $cm^{-1}$ confirms this fact – adsorbed O atoms make the surface phonon dipole-active, so a drop in its intensity is correlated with a drop in O atom adsorption.

Above 0.21 ML Au, loss intensity appears near 750–950 $cm^{-1}$. By 0.25 ML Au, two loss features centered near 760 and 855 $cm^{-1}$ clearly intensify with increasing Au coverage. Beyond 0.33 ML, a well-developed shoulder appears near 960 $cm^{-1}$. These three features originate from molecular $O_2$ adsorbed on at least 3 different sites. Their intensities are further enhanced beyond 0.4 ML Au. Similar frequencies have been seen for molecular $O_2$ adsorbed on Pd, Pt, and Ag as stated in the introduction.

These adsorbates are peroxo- or superoxo-like species with bond orders less than 2 ($O_2^{2-}$ or $O_2^{1-}$, respectively). Above 0.51 ML Au, the loss features near 740, 855, and 960 $cm^{-1}$ drop in

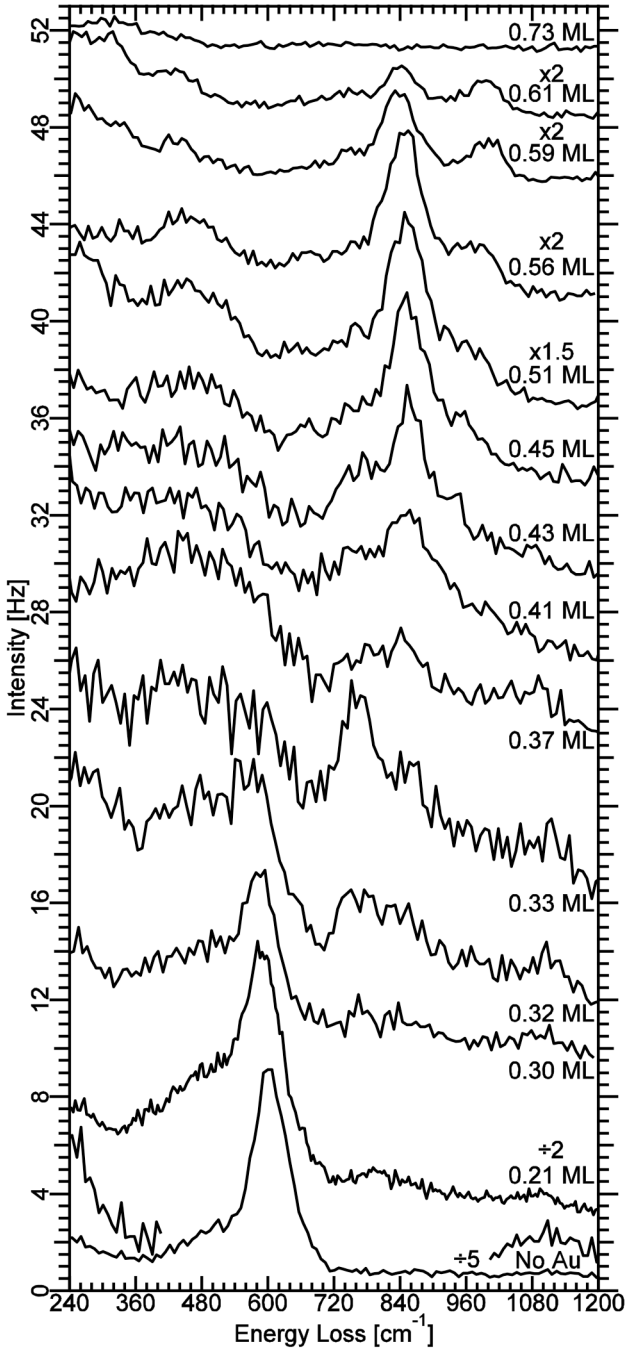


Figure 5. HREELS of $O_2$ on Au-Ni(111) surfaces as a function of Au coverage.

intensity and the highest frequency mode, 960 $cm^{-1}$, blueshifts, reaching about 990 $cm^{-1}$ at 0.61 ML Au. This trend likely indicates extensive weakening of the surface-$O_2$ interaction. Above 0.61 ML Au, the intensities of all loss features reduce further as the $O_2$ adsorption probability approaches that of a pure Au surface. No loss features are observable by 0.79 ML Au (not shown), consistent with 0.80 ML Au being equivalent to a uniform and hexagonally close packed layer of Au atoms adsorbed on Ni(111).

Loss features below 550 $cm^{-1}$ are also changing. At no Au deposition, the low frequency shoulder at 480 $cm^{-1}$, attributed to a "bulk-like" Ni-O stretch[36] (but which might be the antisymmetric Ni-O surface vibrational stretch modes), is less intense than the primary loss feature at 600 $cm^{-1}$. The shoulder becomes more prominent and its maximum shifts to a lower frequency as the Au coverage increases. These loss features predominate beyond 0.33 ML Au and occur in tandem with the appearance of loss intensities above 740 $cm^{-1}$ and the disappearance of the Ni-O symmetric stretch mode. Therefore, these low-frequency loss features are likely a combination of Ni-$O_2$ stretch modes and Ni-O stretch modes reduced in frequency by the presence of Au. The former predominates at high Au coverage, and the latter at low Au coverage. Resolved above 0.61 ML Au are two low frequency features centered near 310–330 $cm^{-1}$ and 435 $cm^{-1}$ that we speculate to be surface-$O_2$ stretch modes, or frustrated rotational or translational modes of adsorbed $O_2$ characterized by the 830–840 $cm^{-1}$ and 990–1000 $cm^{-1}$ stretch modes. We pursued off-specular measurements of all loss features to characterize each of their electron scattering mechanisms, but not enough data were collected to assign the lower-frequency loss features.

Finally, with no Au exposure, a weak-intensity overtone is seen centered at 1120 $cm^{-1}$ whose fundamental is the 600 $cm^{-1}$ Ni-O symmetric stretch. Surprisingly, its intensity is inversely

correlated with the fundamental below 0.33 ML Au. At 0.37 ML, Au the overtone feature is present even when the fundamental is not seen. Moreover, the overtone frequency downshifts to 1080 $cm^{-1}$ just as the Au coverage rises to 0.4 ML. These peculiarities of the 1080–1120 $cm^{-1}$ band suggests the existence of yet another adsorbed molecular $O_2$ species near these frequencies. Generally speaking, HREEL spectra of oxygen adsorbates between 0.3–0.4 ML Au had low intensity and were tremendously difficult to reproduce, as these surfaces were acutely sensitive to contaminants and Au deposition inhomogeneities.

In summary, the HREEL spectra in Figure 5 show the presence of at least 3 (if not 4) distinct cohorts of stable molecular $O_2$ species on Au-Ni surface alloys. The distinct bands of vibrational loss features show that all oxygen species adsorb within just a small family of adsorption sites. Their relative populations are a strong function of Au coverage as small changes in Au coverage result in marked differences in loss features (Figure 5). The evidence is clear that the oxygen–surface interaction is substantially different on alloy surfaces compared to Ni(111). Apparently, Au atoms remove sites that accommodate $O_2$ dissociative adsorption resulting in adsorbed O atoms and simultaneously introduce new sites that support molecular chemisorption unknown on the native Ni(111) surface. These observations are rationalized in the discussion section.

**A. Center Frequencies and Intensities' Au Coverage Dependence**. To understand how the vibrational loss features' center frequencies and intensities change with Au coverage, we fit three Gaussian functions to HREEL spectra in the 700–1200 $cm^{-1}$ energy range that were measured above 0.48 ML Au. The fit is constrained such that the FWHM of the three Gaussians are identical. The same fitting strategy[37] is used on spectra measured below 0.48 ML Au, but with an additional Gaussian function to account for the extra loss feature near 1100 $cm^{-1}$. The FWHM of this fourth Gaussian is allowed to vary independently of the other three. A constant

background is assumed in all fits, with the exception of those below 0.22 ML Au where a linear background is used. No further attempt is made to correct for the very intense loss features between 500–600 $cm^{-1}$ that bleed into the spectral region of interest. Typical fits are shown in Figure 6, with plots of the frequencies and intensities determined from the fit shown in Figures 7

and 8, respectively.

In all fitted spectra, there is evidence of an additional oxygen vibrational feature near 660–680 $cm^{-1}$ outside the fitting interval whose center frequency is coincident with the Au-O stretch observed for O atoms on Au(111).[38] However, its intensity relative to the elastic feature is

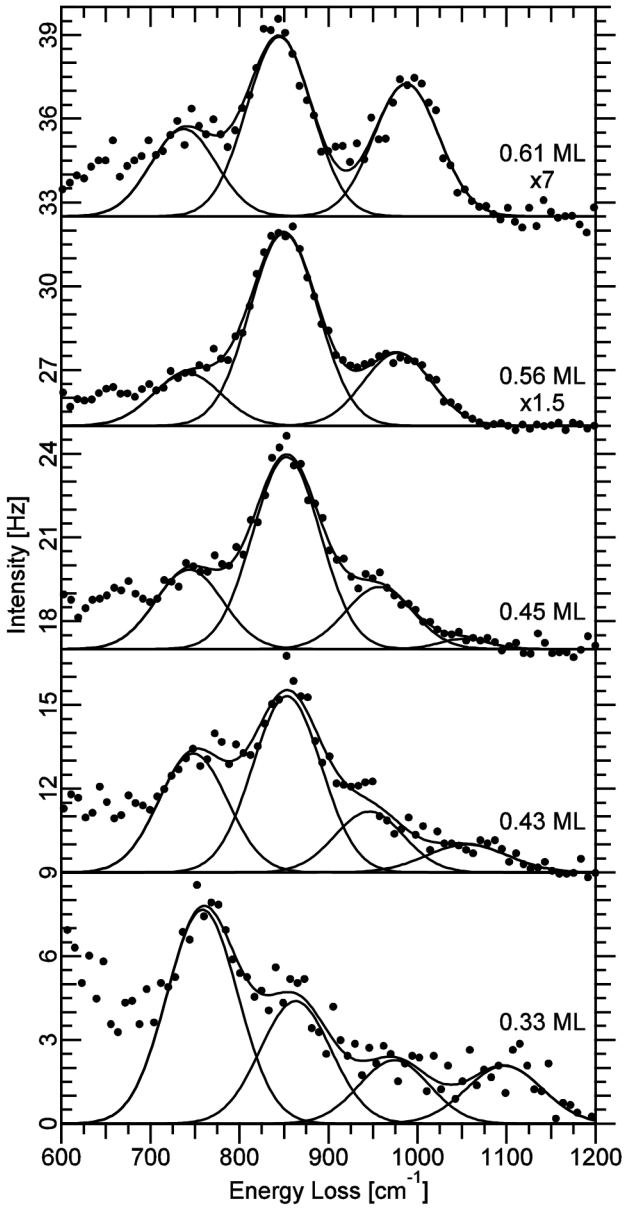


Figure 6. Gaussian fits (see text) to loss features in Figure 5 show loss features change with Au coverage.

enhanced in the limited number of spectra measured at an off-specular angle, which is behavior more consistent with an $O_2$ stretch. More data are needed to assign this weak spectroscopic feature.

The FWHM of the features fit to each spectrum between 0.33–0.61 ML Au are on average 1.6 times broader than the elastic feature. Hence, each vibrational band is actually a convolution of several vibrational modes; additional features could not be identified via further deconvolution. The broadening is likely caused by a distribution of slightly different $O_2$ adsorption sites. Yet, it is clear that these slightly different adsorption sites result in vibrational losses that group into three or four bands over a large Au coverage range. Plotted as a function of Au coverage in Figure 7 are the center frequencies of the vibrational loss features near 740, 855, and 960 $cm^{-1}$ from Figure 5. The error bars at each coverage measurement are equal to plus or minus two standard deviations, as calculated by the fitting routine. The fits and inferred trends in HREEL spectra above 0.4 ML Au are more reliable because intense molecular oxygen loss features superimpose on an unambiguous constant background at these coverages, leading to lower fitting uncertainties and smaller vertical error bars. Larger fitting errors occur below 0.4 ML Au as there are unresolvable loss features centered near 960 $cm^{-1}$ and 1050 $cm^{-1}$. The data collected in this range are too sparse to determine if the center frequencies are sensitive to Au coverage. The prediction intervals for all center frequencies are quoted at the 95% confidence level.

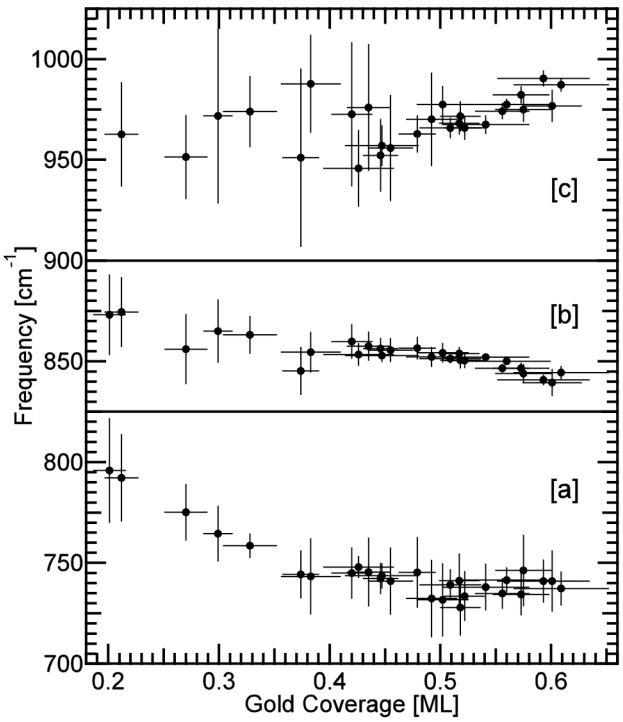


Figure 7. The center frequency of the most prominent $O_2$ loss features are dependent on Au coverage. All error bars are two standard deviations.

The lowest frequency shoulder fitted in Figure 6 is prominent around 760 $cm^{-1}$ at 0.33 ML Au and has a center frequency that decreases to 743 ± 3 $cm^{-1}$ at 0.46 ML Au in Figure 7a. At the same time, the Ni-O stretch at 600 $cm^{-1}$ with no Au exposure shifts to 560 $cm^{-1}$ around 0.33 ML Au (Figure 5). The frequency shifts likely indicate that binding sites are very sensitive to the local environment below 0.33 ML Au.

Similarly, the most prominent loss feature is centered at 856 ± 3 $cm^{-1}$ at 0.46 ML Au. This band is the quintessential peroxo-like loss feature seen on nearly all Au-Ni surfaces studied. In Figure 7b, its center frequency appears to drop gradually with increasing Au coverage, although more data are needed to confirm this trend. In contrast to the band near 743 $cm^{-1}$, the derivative of the plot of frequency versus Au coverage does not change abruptly, indicating that the binding sites for molecular $O_2$ have different sensitivities to Au coverage.

Finally, based on a weighted linear fitting of data points above 0.4 ML Au, the highest-frequency loss feature has a center frequency of 957 ± 5 $cm^{-1}$ at 0.46 ML Au in Figure 7c. Its frequency rises from 945 to 990 $cm^{-1}$ as the Au coverage rises from 0.41 to 0.61 ML (Figure 5), indicating that the higher frequency losses correlate with higher densities of Au atoms. The feature is not detectable by HREELS above 0.66 ML Au (not shown). This observation reflects the weakening $O_2$-surface interaction.

Plotted in Figure 8 are the integrated absolute intensities obtained by integrating the fits to each loss feature (analogous to those in Figure 6) at a given Au coverage. The data points

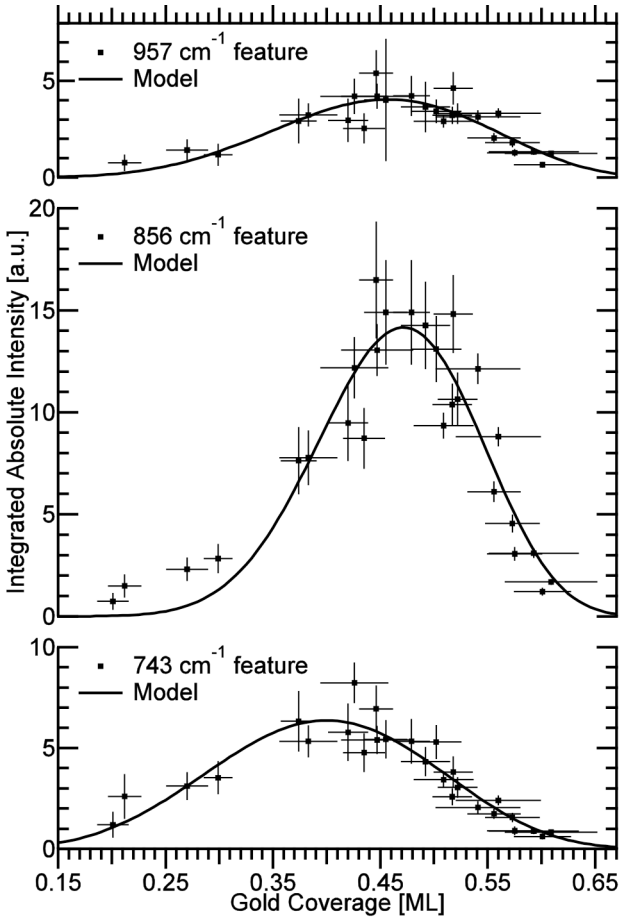


Figure 8. Integrated absolute intensities of the three major molecular $O_2$ loss features as a function of Au coverage. All error bars are two standard deviations.

represent integrated absolute intensities of each $O_2$ cohort and are assumed to be proportional to coverage. The solid lines are guides to the eye based on a fitting ansatz and all error bars are two standard deviations. These values are used to calculate the population fraction of each $O_2$ species, defined as the integrated intensity of each loss feature divided by the sum of the integrated intensities of each loss feature at a given Au coverage. These population fractions are shown in Figure 9 and vary with Au coverage differently compared to the trends shown in Figure 8. In particular, the integrated absolute intensity maxima and the population fraction maxima do not occur at the same Au coverage. For example, the population fraction of $O_2$ whose band is centered at 743 $cm^{-1}$ at 0.46 ML Au is highest at its detection threshold near 0.2

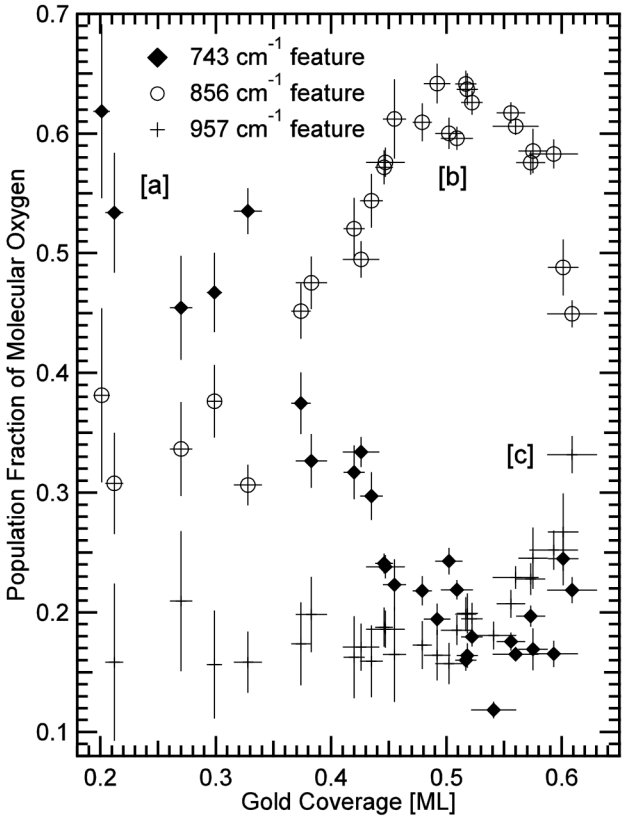


Figure 9. Population fractions of the three major molecular $O_2$ species calculated with absolute intensities that are assumed to be proportional to coverage. All error bars are one standard deviation.

ML Au (Figure 9a), even though its loss feature intensity is not clearly seen until 0.33 ML Au (Figure 5). A similar (but much weaker) effect is seen for the 856 $cm^{-1}$ feature whose population fraction peaks slightly above 0.5 ML Au (Figure 9b) although its total integrated intensity saturates slightly below at 0.46 ML Au. By extrapolation, the population fraction of the 957 $cm^{-1}$ feature becomes the majority species around 0.62 ML Au (Figure 9c). In summary, the population fractions for the 743, 856 and 957 $cm^{-1}$ loss features are maximized near 0.2, 0.5, and above 0.6 ML Au respectively.

There are additional trends present in Figure 9 that warrant further analysis. With only one exception, the population fraction of each $O_2$ species never dips below 0.15. This lower limit is an artifact of assuming that all loss features have constant background contributions. It also appears that $O_2$ adsorption is differently sensitive to changes in Au coverage below and above 0.5 ML. Below this coverage, the population fraction of the 856 $cm^{-1}$ loss feature increases at the expense of the 743 $cm^{-1}$ loss feature, while the 957 $cm^{-1}$ loss feature stays constant. Only above 0.5 ML Au do all three population fractions change simultaneously with Au coverage.

In the high Au coverage regime, the population fraction of molecular $O_2$ centered at 957 $cm^{-1}$ increases appreciably. The center frequency of this feature shifts to nearly 1000 $cm^{-1}$ above 0.6 ML Au. Occurring in tandem is a possible rise in the relative fraction of the lower frequency 743 $cm^{-1}$ feature that is accentuated in a barycentric plot (not shown). Nevertheless, the dominant trend is that lower or higher Au coverage favors molecular $O_2$ adsorption with respectively lower or higher $O_2$ stretch frequency.

For completeness, Figure 10 shows the total integrated loss intensities of molecular $O_2$ as a function of Au coverage. These values were obtained by summing the integrated intensities of the 743, 856, and 957 $cm^{-1}$ loss features in Figure 6 at each Au coverage. The solid line is a sum

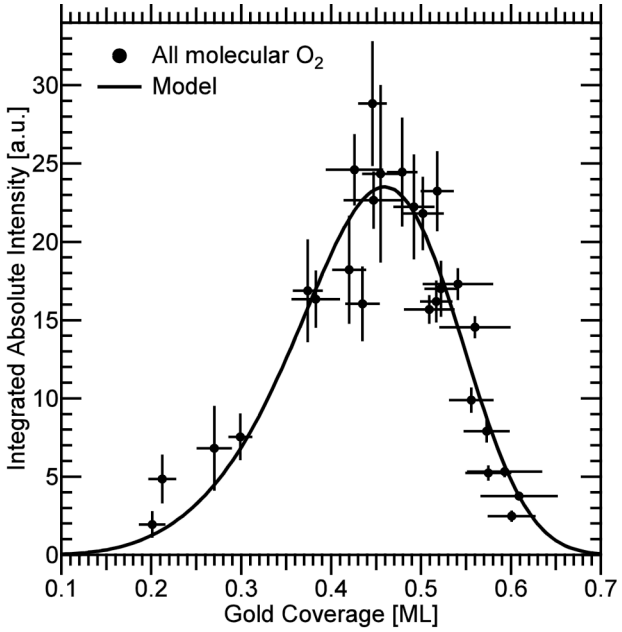


Figure 10. Sum of integrated intensities of the 743, 856, and 957 $cm^{-1}$ loss features. See text for explanation of solid line. All error bars are two standard deviations.

of the three model fits shown in Figure 8. According to the fit, adsorption of molecular $O_2$ is highest near 0.46 ML Au and tapers off as the Au coverage deviates from this optimum value. At 0.46 ML Au, where the total molecular $O_2$ intensity is a maximum, the relative population of 957, 743, and 856 $cm^{-1}$ loss features is nearly in the ratio of 1:2:5 whose physical origin is discussed later.

**B. Absolute Oxygen Atom Coverage Estimates**. Information on the absolute O atom coverage on Au-Ni surfaces is determined via Auger spectroscopy by measuring the ratio of O (510 eV) to the sum of Au (74 eV) and surface Ni (849 eV) Auger intensities, with sensitivity factor corrections for all Auger transitions. Very importantly, this O atom coverage assignment method is consistent with absolute O atom coverage assignments obtained using an independently obtained calibration factor of 0.8168 $ML^{-1}$. Above 0.59 ML Au the amount of oxygen adsorption (still detectable by HREELS) drops below the detection limit of the Auger spectrometer.

Auger measurements show that the total surface O atom coverage drops monotonically with increasing Au coverage (Figure 11). Just under 0.40 ML O atoms adsorb at 0.17 ML Au coverage, therefore putting an upper bound of 0.20 ML $O_2$ molecules that can be accommodated on all alloy surfaces. Near 0.46 ML Au, molecular $O_2$ vibrational loss features attain their highest intensity and no atomically bound O atoms are detected near 580 $cm^{-1}$. Consequently the surface is covered predominantly with molecularly bound $O_2$. These observations indicate that surface Au atoms convert sites for dissociative chemisorption to molecular adsorption in tandem with removing adsorption sites. At 0.46 ML Au, nearly 0.11 ML O atoms are adsorbed (Figure 11) so about 0.055 ML $O_2$ molecules are present molecules are present or about $0.055 \div 3 \approx 0.018$ ML per cohort. At this concentration, the average distance between each $O_2$ molecule is 4–5 nearest neighbor surface atoms and their spatial separation is large enough that their pairwise interactions are weak, if not negligible. Hence, these $O_2$ coverage estimates seem rather low as

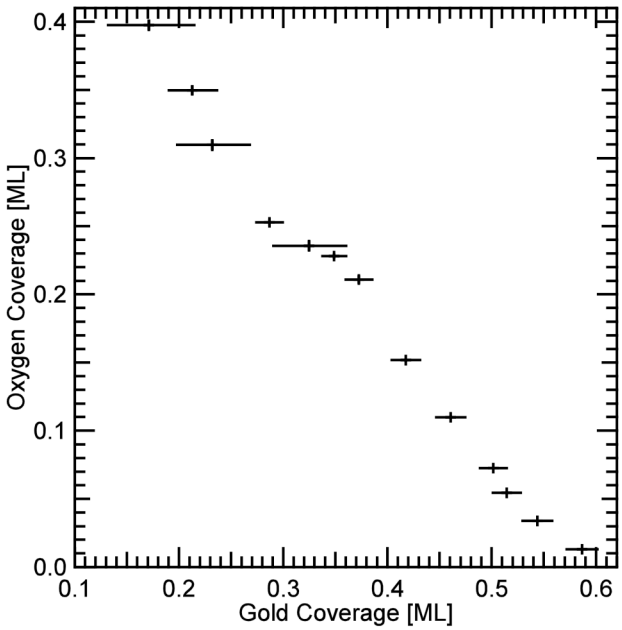


Figure 11. Oxygen coverage in ML of O atom per Ni atom measured by Auger electron spectroscopy as a function of Au coverage. Error bars are two standard deviations.

even a single unit cell appears large enough to accommodate much more oxygen (Figure 3). On the other hand, much of the surface is already passivated by Au above 0.46 ML Au, making it likely that the $O_2$ species are corralled into Ni dominated surface areas by Au atoms. Experiments probing the spatial distribution of the adsorbed $O_2$ would answer this question.

Across the entire range of Auger measurements, the oxygen coverage when measured as monolayers of O atoms per surface atom (Figure 11) decreases almost linearly with increasing Au coverage, despite the very complex surface alloy phase transition occurring between 0.3–0.4 ML Au. A close look reveals a small sigmoidal trend present between 0.25–0.40 ML Au that coincidentally brackets this interval. Absent of a direct counting method for O and Au coverage determination, it is an open question whether this sigmoidal feature truly reflects complex surface restructuring or is an artifact of our particular O and Au coverage assignments. The slope of a best fit line through data points between 0.2–0.6 ML Au show that each Au atom incorporated into the Ni(111) lattice prevents 0.92 O atoms from adsorption. The proximity of this slope to unity shows the effectiveness of Au atoms in quenching the surface oxidation of Ni(111). It suggests that each Au atom incorporated into Ni(111) removes one binding site for an oxygen atom. This interpretation is consistent with our observations that no oxygen adsorbs on the 0.8 ML Au saturated Ni(111) surface. As a precautionary note to future studies, we have found that the O atom coverage is greatly perturbed by slight C contamination, an effect that is corroborated with spurious effects in both Auger and HREELS data.

## V. DISCUSSION

We begin with an empirical observation involving the oxygen adsorbate binding energy[39] and the activation barrier for $O_2$ dissociation on metal surfaces. Through extensive DFT calculations[40], it

has been shown that a direct, linear relationship exists between these two quantities,[41] where an increased activation energy for dissociative chemisorption coincides with a decreased interaction strength between the surface and the adsorbed oxygen moiety. This activation barrier is largely determined by the energy difference between the Fermi level and the valence d-band center, with larger differences corresponding to higher barriers. If the Fermi level is used as a fixed energy reference across all surface alloys, the addition of Au to Ni(111) will decrease the energy of the d-band center. The physical origins of this decrease are explained later.

Since the experimental barrier to $O_2$ dissociative chemisorption is nearly absent on Ni(111)[9] and between 1.0–1.3 eV on Au(111)[42], these two metal surfaces have d-bands whose centers are respectively close and far from the Fermi level. Therefore, an alloy of the two metals might have an intermediate d-band center depth whose surface-$O_2$ interaction results in an intermediate value for the $O_2$ dissociative chemisorption barrier. In this situation, the probability of dissociative adsorption of $O_2$ is suppressed while the probability of molecular $O_2$ adsorption is enhanced. The identification of peroxo- and superoxo-like vibrational bands measured by HREELS in Figures 4 and 5 supports this perspective and highlights the utility of a surface vibrational spectroscopy technique for categorizing new chemisorbed states. In contrast, assuming chemical inertness of Au can lead to the incorrect hypothesis that its incorporation into the Ni(111) lattice just passivates the Ni surface without any resulting chemical novelty. The unusual molecular $O_2$ chemisorption states observed in this work are not due to single Au atoms, nor dispersed Au clusters, nor Au nanoparticles resting on Ni(111). Rather, they result from emergent properties or ensemble effects of a bimetallic random surface alloy whose distinguishing properties can be explained with a combination of electronic structure and geometrical arguments.

**A. Electronic Structure of the Surface Alloy**. The salient features of the alloy d-band

include its average energy (or "center"), bandwidth, and filling extent. Systematic changes in these quantities describe chemisorptive trends across all transition metals and their alloys. Since these quantities change in a strongly correlated manner[43], it suffices to use just one as a representative descriptor of surface reactivity. The d-band center is a convenient choice because the presence of a Fermi level constrains the d-band center to shift in response to changes in filling and orbital interactions in the alloy. Here, the Fermi level is a fixed energy reference for all alloy surfaces because the d-band characterization is done at thermodynamic equilibrium.

The chemisorption strength decreases as one traverses the transition metals in the periodic table in both top-to-bottom and left-to-right fashion.[43] The former is attributed to the presence of increasingly diffuse 3d, 4d, and 5d orbitals that increases the surface-adsorbate repulsion for fixed surface-adsorbate geometry. The latter is dominated by increased d-band filling which increases the occupation of antibonding states. Since Au is to the right and below Ni on the periodic table, both prevailing trends align so that the chemisorptive tendencies of the Au-Ni alloy surface would be weaker than a pure Ni surface. Overall, substituting Au atoms into the Ni(111) lattice causes the d-band to decrease in average energy, increase in width, and negligibly increase in filling. The significance of these terms will be discussed presently.

The d-band center is lowered because the Au 5d electrons in Au metal form[14] two deeply bound bands about 4 and 6 eV below the Fermi level, which places them respectively nearly 3 and 5 eV below the Ni 3d band. The surface electronic structure of Ni(111) is drastically modified by the addition of Au because the lower energy Au 5d electrons substitute for Ni 3d electrons present in the original Ni valence 3d band, thereby lowering the d-band center energy substantially and diluting the Ni 3d electron density at the surface. For instance, it has been calculated that isolated Au atom impurities in Ni(111) and a complete Au overlayer on Ni(111)

decrease the 1.29 eV Ni 3d band center by a further 1.13 eV and 2.10 eV respectively[43]. These calculations show that surface alloy electronic structure is substantially different from its parent metals in isolation.

The physical origin of the increased d-band width is understood by considering a fictitious collection of Ni atoms infinitely far apart. In this scenario, the d-band has zero width as the 3d orbital energies are completely degenerate. Once the Ni atoms are brought together to form a Ni crystal, mixing of the 3d orbitals spreads the 3d orbital energy levels and leads to a d-band of finite width. Qualitatively, the bandwidth is proportional to the degree of d-orbital hybridization. Both can be simultaneously increased by compressively straining the Ni surface, which in fact, is exactly the effect of alloying the larger Au atoms into the Ni(111) lattice below 0.3 ML Au. Above this coverage, some compressive surface strain is released by the surface reconstruction and increased effective lattice constant, but not enough to reverse the trend that increasing Au coverage causes the d-band to widen. It is also true that the Au 5d band widens in the alloy at all Au coverages because the surface Au atoms rest closer to its neighboring atoms (either Au or Ni) than they do in Au(111). It should be stressed that since the effective atomic size of Au exceeds Ni, the compressive strain of Ni atoms resting beside Au atoms leads to d-band broadening even in the absence of hybridization between Au and Ni atom d-states. This broadening is also favored because Ni is a 3d transition metal with one of the highest atomic numbers, and therefore, a metal with one of the most compact set of d-orbitals. Any other transition metal possesses more diffuse d-orbitals (with the Cu and Zn being exceptions) so the d-band will tend to widen when incorporated into the Ni lattice.

To isolate the impact of increased d-band filling on the d-band center, consider a fictitious valence d-band with a fixed density of states distribution and width, negligibly populated with

electrons. The energy level of these electrons is nearly degenerate and coincides with the Fermi level. However, the d-band center and the empty d-states lie above the Fermi level. As the d-band filling fraction increases, the empty states fill and shift below the Fermi level. The location of the d-band center with respect to the Fermi level decreases and changes sign around the point when the d-band is half full. Afterwards, the d-band center will lie below the Fermi level and within the populated density of states. These general trends are seen when moving from left to right across the transition metals as the d-orbitals are progressively populated.

In the case of Ni, its d-band is already 90% (and nearly completely) filled. Hence, the existing population of surface-$O_2$ antibonding states is quite high, meaning that the extent of surface adsorbate stability attributable to d-band filling is relatively low[44]. When Au is incorporated into Ni(111), Au $d^{10}$ orbitals replace Ni $d^9$ orbitals, which is predicted to raise the d-band filling. Changes in the d-band filling would indicate charge transfer from one metal to another involving the d-states. However, strong coulombic repulsions arising from converting Ni $3d^9$ to Ni $3d^{10}$ states counter this effect and so the filling remains practically unchanged. Empirical DFT calculations[45] of various bilayer surfaces made of 3d and 5d metals suggest this approximation is reasonable, and is supported by photoelectron experiments on Au-Ni surfaces.[14] The DFT result is not surprising given that the electronegativity of the transition metals is well matched. However, as Au is the most electronegative of metals, it is clear that the full description of the Au-Ni alloy requires much more sophistication. For example, charge transfer may still take place amongst other combinations of orbitals[14] and affect the surface chemistry of the alloy. Nevertheless, since the d-band filling remains approximately constant even after alloying, the correlation of the lowering of the d-band center with d-band widening in a nearly one-to-one manner[45] is ensured. This effect reduces the density of electrons at the Fermi level

available for overlap with the $O_2$ $\pi^*$ orbitals and lowers the dissociative chemisorption probability.

**B. $O_2$ Interactions with the Surface Alloy**. Consider the interaction of molecular $O_2$ with the Ni(111) surface, most conveniently modeled as two interaction steps.[46] The first step involves the Ni 4s band and the highest partially occupied molecular orbital (HOMO) of $O_2$, which is the antibonding $\pi^*$ orbital. The second involves the result of this first interaction and the Ni 3d band. Hybridization between the $\pi^*$ state and the Ni 4s band results in a broadened and more stable, lower energy $\pi^*$ band. The center of this new $\pi^*$ band is at a lower energy than the original $\pi^*$ state because the $\pi^*$ state is formed from two atomic oxygen 2p states that are lower energy than the Ni 4s band. The $\pi^*$ and Ni 3d bands then interact and form new bonding and antibonding $\pi^*$–3d bands that reside below and above the Fermi level, respectively.

The states above the Fermi level are essentially unoccupied, so the stability of molecular $O_2$ on Ni(111) is largely governed by the strength of the bonding $\pi^*$–3d interaction[35]. Other bands that arise from the bonding molecular orbitals of $O_2$ are ignored in this approximation because they are situated 6 eV below the Fermi level[10]. A stronger $\pi^*$–3d interaction enables filling the $\pi^*$ band with 3d electrons, weakening the $O_2$ double bond and causing it to lengthen, and leads to dissociative chemisorption of $O_2$ on Ni(111) and eventually, adsorption of atomic O in fcc 3-fold hollows. A weaker $\pi^*$–3d interaction suppresses this dissociative channel.

The strength of this $\pi^*$–3d interaction is inversely proportional[44] to the energy difference between the centers of the $\pi^*$ and 3d bands. Ignoring spin-splitting effects, the $\pi^*$ band is at the Fermi level[10] and the Ni 3d band is 1.21–1.29 eV below it[10, 47]. The position of the Ni 3d band is sufficiently close to the Fermi level that the $\pi^*$–3d interaction is very favorable, hence dissociative chemisorption of $O_2$ on Ni(111) is observed. If the 3d band center were to decrease, the strength of the $\pi^*$–3d interaction would also decrease and eventually lead to molecular $O_2$

chemisorption. If the 3d band center were to decrease even further, it would lead to non-adsorption.

Unlike the smaller 3d orbitals of Ni, the larger 5d orbitals of Au overlap unfavorably with the antibonding orbitals of $O_2$. This overlap reflects the higher energetic cost of overcoming the Pauli repulsion between the adsorbate electrons and the surface made of metal atoms that have more diffuse valence orbitals.[47] This repulsion is a quantum mechanical effect that involves orthogonalization of the diffuse Au 5d orbitals with respect to the adsorbate. As the Au coverage is raised, the unfavorable Au 5d interaction gradually replaces the favorable Ni 3d interaction, leading to the surface–$O_2$ interaction weakening and its d-band center lowering.

Molecules of $O_2$ with bond orders less than 2 are stabilized in these new chemical environments as indicated by their internal vibrational frequencies. While band structure arguments do support these species' existence, they cannot account for the distinct vibrational group frequencies in Figure 5 above 0.33 ML Au because the d-band model ignores the phase transition that occurs above 0.3 ML Au. It is one reason why we introduced a model unit cell that reproduces the known surface morphology at all Au coverages.

**C. Geometric Effects of the Surface Alloy**. Our first attempts at correlating the number and intensity of the vibrational features with molecular $O_2$ adsorption sites on Au-Ni(111) involved tallying all unique adsorption sites found in computer generated Au-Ni unit cells of a single layer of the alloy. We did not find a subset of distinct adsorption sites whose prevalence was proportional to the intensities of the molecular $O_2$ vibrational features for all Au coverages. Hence, the observed distribution of molecular $O_2$ adsorption (Figure 10) could not be reproduced by mimicking the random placement of Au atoms at lattice sites found in the top layer of a real surface alloy. We deduced that $O_2$ adsorption is inadequately described by considering only

surface atoms. Subsurface atoms associated with the second layer reconstruction appear to contribute to the stability of adsorbed $O_2$ based on a careful analysis of molecular $O_2$ HREELS loss intensities combined with recent DFT calculations[48].

Why do only a few distinct environments for oxygen adsorption result from randomly embedded Au atoms in Ni(111)? We think this has to do with the structure of the surface as summarized in our model unit cell (Figure 3). Recall that the total integrated molecular $O_2$ loss intensity is maximized at 0.46 ML Au. At this coverage, the ratio of the intensities of the HREELS loss features centered near 856, 743, and 957 $cm^{-1}$ is about 5:2:1. This ratio matches the relative sizes of three differently shaded regions of the unit cell in Figure 3: non-reconstructed pseudo-2-fold, non-reconstructed pseudo-3-fold, and reconstructed pseudo-3-fold. To a first approximation, this coincidence suggests that distinct molecular $O_2$ features are associated with distinct regions.

On a model 0.25 ML Au surface whose p(2×2) unit cell consists of a $AuNi_3$ cluster, molecular $O_2$ is predicted to adsorb nearly flat and in the vicinity of bridge, hcp 3-fold, and fcc 3-fold sites formed entirely of Ni atoms with adsorption frequencies 932, 768, and 767 $cm^{-1}$, respectively.[48] Adsorption in the bridge position occurs with the $O_2$ center of mass over a bridge site with both O atoms close to atop sites. In the hcp and fcc position, one O atom is close to the 3-fold hollow while the other atom is close to a Ni atom. Since the model consists of four layers with the bulk fixed to match the native Ni(111) crystal, these calculations assume no reconstruction and can only qualitatively reproduce the pseudo-3-fold coordinating regions that comprise 3/8 of our proposed unit cell whose constituent supporting atoms are shaded in Figure 3. Despite these shortcomings, the agreement between theoretical and experimental results suggests a tentative assignment of the observed vibrational bands centered at 957 and

743 $cm^{-1}$ to $O_2$ adsorption within pseudo-3-fold coordinating regions with binding geometries corresponding to the predicted bridge and hcp/fcc site adsorption, respectively.

Notably absent from these DFT calculations is evidence for adsorbed $O_2$ with internal stretch frequencies that match the most intense loss intensity seen at 856 $cm^{-1}$. A possible explanation for the absence of this loss feature is the failure of the slab geometry in the calculation to model the complementary pseudo-2-fold coordinating region that comprises the remaining 5/8 of the unit cell (as indicated by unshaded atoms in Figure 3). If this hypothesis is correct, it allows us to complete the vibrational assignment of the loss feature near 856 $cm^{-1}$ to molecular $O_2$ adsorbed within the pseudo-2-fold coordinating regions of the unit cell. The observation of a single vibrational band suggests that $O_2$ adsorbed at bridge and hcp/fcc sites within pseudo-2-fold coordinating regions of the unit cell have nearly identical internal vibrational stretch frequencies.

We can rationalize this surprising accidental degeneracy by noting that a key distinguishing feature between pseudo-2- and pseudo-3-fold coordinating regions is the presence of subsurface coordinating atoms located immediately underneath a large fraction of bridge and hcp/fcc $O_2$ binding sites, respectively. The atoms in Figure 3 that make contact with the points of perfect 2- and 3-fold rotational symmetry in the pseudo-2- and pseudo-3-fold coordinating regions are canonical examples of this important spatial relationship and are shown in Figure 12a and 12b, respectively. The Wigner-Seitz cells in Figure 12 are hexagonally shaped, and respectively, all

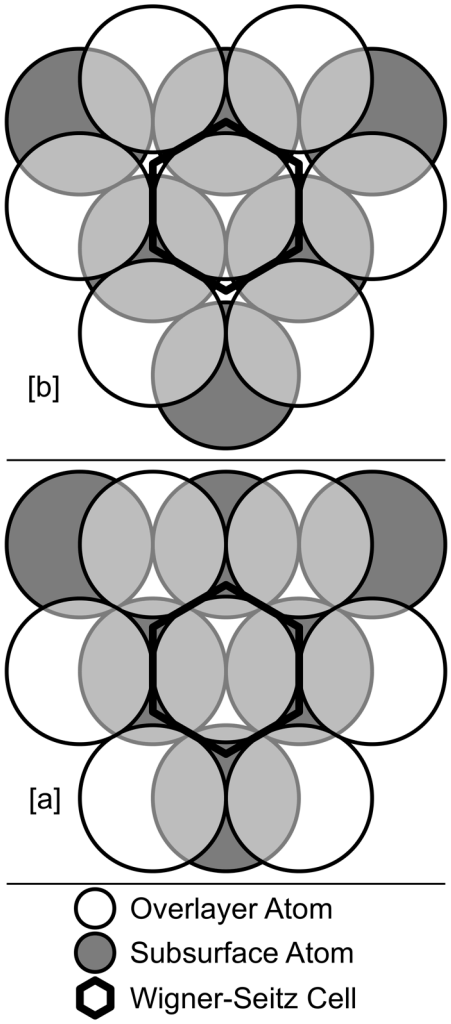


Figure 12: Idealized 2-fold [a] and 3-fold [b] coordination between overlayer and subsurface atoms present in the Au-Ni alloy unit cell.

bridge and hcp/fcc $O_2$ binding sites are coincident with its edge centers and corners. In going from Figure 12a to 12b, it is clear that the subsurface coordination number increases for bridge sites, and decreases for hcp/fcc sites. The higher subsurface coordination number increases the availability of Ni 3d electrons that can overlap with the antibonding orbitals of $O_2$ at those sites. Consequently, when molecular $O_2$ is bound to bridge sites, this overlap is more favorable in pseudo-2-fold rather than pseudo-3-fold coordinating regions. This favorable overlap is clearly

illustrated by the much lower vibrational frequency of bridge-bound $O_2$ within coordinating regions of type pseudo-2-fold (856 $cm^{-1}$) compared to pseudo-3-fold (957 $cm^{-1}$). Similarly, $O_2$ adsorption at hcp/fcc sites results in more favorable overlap within coordinating regions of type pseudo-3-fold (743 $cm^{-1}$) rather than pseudo-2-fold (856 $cm^{-1}$). We propose that the extent of this overlap as one goes from a pseudo-3-fold to a pseudo-2-fold region is coincidentally the right magnitude that leads to the observed degeneracy of the bridge and hcp/fcc threefold binding sites in the pseudo-2-fold coordinating regions of the unit cell.

No abrupt boundaries separate different adsorption regions (except at the reconstruction) as coordination number varies smoothly when crossing from one domain to another. However, this fact appears incommensurate with the nearly 100 $cm^{-1}$ difference in vibrational frequency of adsorbed $O_2$ in pseudo-2-fold and pseudo-3-fold regions. We resolve this discrepancy by assuming that the fraction of adsorption sites bordering different domains is small so that $O_2$ with interpolating vibrational frequencies are in the minority and do not blur the observation of three distinct vibrational bands. In order to determine the relative binding strength of $O_2$ from these cohorts, one could expose the surface at fixed Au coverage to increasing amounts of $O_2$ and watch the lowest energy states fill first. However, we have preliminary evidence based on dilute molecular beam exposures that the binding energies are too similar or the diffusion barriers between binding sites are too small to determine the relative binding energies. For completeness, vibrational bands seen near 660 and 1000 $cm^{-1}$ that do not interpolate between the values of 743, 856, and 957 $cm^{-1}$ are thought to be $O_2$ associated with the reconstruction loop.

The relative populations of differently-adsorbed $O_2$ are non-trivially dependent on the size of the misfit dislocation loop. To illustrate this point, note that the reconstructed and non-reconstructed pseudo-3-fold coordinated regions cover about 1/8th and 2/8th of the unit cell

respectively. By coincidence, the 957 and 743 $cm^{-1}$ molecular $O_2$ species also adsorb in a nearly 1:2 ratio around the molecular $O_2$ adsorption maximum of 0.46 ML Au. Two limiting cases of adsorption behavior are consistent with these observations. Either the 957 and 743 $cm^{-1}$ species adsorb exclusively on the reconstructed and non-reconstructed sections of the pseudo-3-fold coordinated regions respectively, or in a fixed 1:2 ratio in both. However, neither of these adsorption models are correct because they cannot explain the variance in adsorption trends in Figure 8 as a function of Au coverage. More importantly, these models ignore the likely fact that the ratio of 957 to 743 $cm^{-1}$ species should be higher within the reconstruction because the triangular misfit dislocation loop surrounds the molecules adsorbed inside it. This drastic removal of 3d-electron density at the reconstruction boundary induces weaker surface–$O_2$ interactions that preferentially favor the weaker bound, higher frequency 957 $cm^{-1}$ species with increasing Au coverage.

The explanation for why the 957 to 743 $cm^{-1}$ species ratio does not remain 1:2 across all Au coverages appears related to finite-size effects near the reconstruction boundary. If $p$ denotes the periodicity of the unit cell, the number of surface atoms that rest near the boundary is proportional to $p$. Since $p^2$ is the number of surface atoms in a unit cell, the fraction of atoms affected by the loop per unit cell is proportional to $1/p$. Since this loop atom fraction is small at low Au coverage, the number of adsorption sites perturbed enough by the loop to stabilize the weaker bound 957 $cm^{-1}$ species is low. Consequently, at low Au coverages, the features centered near 743 $cm^{-1}$ predominate and the relative fraction of 957 to 743 $cm^{-1}$ species is less than the predicted 1/2. Once the Au coverage is sufficiently high, the perturbations are strong enough that the 957 $cm^{-1}$ feature is prominent and the relative fraction of 957 to 743 $cm^{-1}$ species is greater than the predicted 1/2. In other words, the ratio of 957 to 743 $cm^{-1}$ species changes with

Au coverage because both species are affected by the relative fraction of loop atoms present in the unit cell at that Au coverage. As no reconstruction occurs below 0.3 ML Au, this argument no longer holds as no loop atoms are present. Instead, the absence of 957 $cm^{-1}$ adsorption in this regime is due to the relatively high energy of the alloy d-band center.

The $O_2$ loss features are broad primarily due to variations in the chemical environment caused by randomly distributed Au atoms at the surface. There is a smaller effect caused by differently coordinated subsurface atoms that is easiest to describe for the pseudo-3-fold coordinating regions of the unit cell. First, denote the letters A, B, and C to represent the three unique [111] stacking layers that make up a fcc crystal. The canonical stacking pattern starting from the top is **AB**CAB and describes the pseudo-3-fold coordinated region of the unit cell furthest from the reconstruction (Figure 3). However, due to lattice mismatching, **CB**CAB stacking is found at the unit cell corners with surface atoms residing in hcp instead of fcc sites. Finally, a palindromic **BA**CAB stacking is found within the reconstruction. Here, subsurface atoms reside in hcp instead of fcc sites. The reconstruction is crucial to this stacking as it cannot arise by lattice mismatching alone. Smaller contributions to $O_2$ loss feature broadening occur because different stacking patterns exist within the unit cell. Overall, a qualitative description of molecular $O_2$ adsorption trends that elegantly accommodates both electronic and geometric effects can be achieved with our model unit cell (Figure 3). The spatial arrangement of atoms near the surface helps explain the peculiar distribution $O_2$ loss intensities as a function of Au coverage seen by HREELS.

This description of the effective unit cell that highlights the first two surface layers is a significant improvement over previous single-layer mean field models of the Au-Ni(111) surface.[29] Our model is a realistic representation of the average electronic and geometric

structure of the areas of Ni atoms that are surrounded by Au atoms. Future refinements based on knowing the exact spatial arrangement of individual Au and Ni atoms can be easily accommodated.

## VI. CONCLUSIONS

Despite the importance of molecular $O_2$ in many heterogeneous catalytic reactions, vibrational studies of molecular $O_2$ on metal surfaces are uncommon, as discussed in the introduction. The rarity of model metal-containing systems that stabilize molecular $O_2$ observable under ultra-high vacuum limit our understanding of these chemical intermediates. Our analysis of molecular $O_2$ adsorption on bimetallic Au-Ni surface alloys resulted in the identification of unique chemical environments that stabilize molecular $O_2$ and extended the number of model systems available for their study. Most importantly – and in tandem with a separate study – our work affirmed a possible connection between the geometry of the very complex reconstructed surface, and the adsorption sites of $O_2$ that oxidize CO at some of the lowest recorded temperatures. It is significant because a complete description of the elementary step reactions for CO oxidation in the same system requires detailed knowledge of the molecular $O_2$ intermediate.

The adsorbed $O_2$ molecule is distinctly sensitive to the surface environment due to strong interactions between its antibonding molecular orbitals and the metal d-band. These electronic effects (inseparable from geometric considerations) account for the distinct vibrational bands identified as molecular $O_2$. No evidence for physisorbed oxygen was found. At 0.46 ML Au, where the intensities of these loss features are maximized, three intense bands with center frequencies at 743, 957 and 856 $cm^{-1}$ are seen (often accompanied by other unidentified minority species at 660–680 $cm^{-1}$ and 1080–1120 $cm^{-1}$). They correspond to the stretch vibrational mode of $O_2$ at pseudo-3-fold fcc/hcp, pseudo-3-fold bridge, and degenerate pseudo-2-fold fcc/hcp and

bridge adsorption sites respectively. These unusual sites are brought about by surface alloying and further stabilized by a dramatic reconstruction of the top two surface layers. This observation is a key result because it is not obvious that the spatial arrangement of substrate atoms relative to the top layer should contribute greatly towards modifying the electronic states of the surface! By measuring vibrational loss features as a function of Au coverage, we show that the relative population of different oxygen cohorts can be tuned. This ability to adjust the reactivity and concentration of surface-bound $O_2$ raises the utility of surface alloy motifs for engineering applications.

The novelty of this work rests on the very counterintuitive observation that the addition of a passivating material such as Au to a chemically active surface like Ni can result in a new surface with reactivity greater than either of its native constituents. Our observed vibrational features unequivocally demonstrate the formation of new chemical environments. Moreover, these environments are distinct from motifs that result from the deposition of Au nanoparticles on metal oxides. In our study, it is not the interface of the gold and nickel oxide that brings about new chemistry. Rather, it is changes in the surface electronic structure brought about by the mutual interaction of Au and Ni atoms that enhance the stability of $O_2$ on the surface.

As our experimental methods do not probe electronic structure directly, further work is necessary to clarify the true nature of oxygen binding sites in Au-Ni surface alloys. We hope our proposed unit cells will be helpful to both theorists and experimentalists alike. The most intense molecular $O_2$ loss feature centered at 856 $cm^{-1}$ seems to be characteristic of the reconstructed surface. A direct confirmation that it is indeed associated with pseudo-2-fold coordinated surface atoms should be a challenging but worthwhile pursuit. We welcome others to continue exploring this enigmatic adsorption system.

## AUTHOR INFORMATION

[+]Current affiliation: Lam Research Corporation

[*]stceyer@mit.edu, Phone: (617) 253-1801

## ACKNOWLEDGEMENTS

This research was supported by DoE, DE-FG02-05ER15665 and by the Shell-MITEI Seed Fund Program. C. C. Leon thanks the Natural Sciences and Engineering Research Council of Canada for a Postgraduate Scholarship PGS D3-374322-2009.

## Table of Contents Graphic

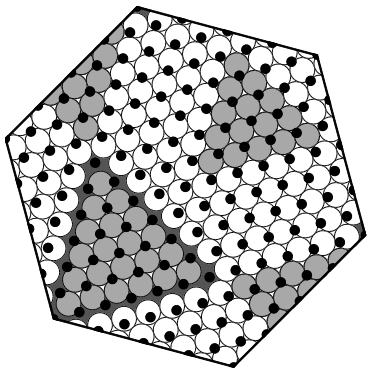

## REFERENCES


(1) Imbihl, R.; Demuth, J. E. Adsorption of Oxygen on a Pd(111) Surface Studied by High Resolution Electron Energy Loss Spectroscopy (EELS). *Surf. Sci.* **1986**, *173*, 395–410.

(2) Kolasinski, K. W.; Cemic, F.; Hasselbrink, E. $O_2$/Pd(111). Clarification of the Correspondence Between Thermal Desorption Features and Chemisorption States. *Chem. Phys. Lett.* **1994**, *219*, 113–117.

(3) Nolan, P. D.; Lutz, B. R.; Tanaka, P. L.; Mullins, C. B. Direct Verification of a High-Translational-Energy Molecular Precursor to Oxygen Dissociation on Pd(111). *Surf. Sci. Lett.* **1998**, *419*, L107–L113.

(4) Gland, J. L.; Sexton, B. A.; Fisher, G. B. Oxygen Interactions with the Pt(111). *Surf. Sci.* **1980**, *95*, 587–602.

(5) Steininger, H.; Lehwald, S.; Ibach, H. Adsorption of Oxygen on Pt(111). *Surf. Sci.* **1982**, *123*, 1–17.

(6) Avery, N. R. An EELS and TDS Study of Molecular Oxygen Desorption and Decomposition on Pt(111). *Chem. Phys. Lett.* **1983***, 96*, 371–373.

(7) Nolan, P. D.; Lutz, B. R.; Tanaka, P. L.; Davis, J. E.; Mullins, C. B. Molecularly Chemisorbed Intermediates to Oxygen Adsorption on Pt(111): A Molecular Beam and Electron Energy-Loss Spectroscopy Study. *J. Chem. Phys.* **1999**, *111*, 3696–3704.

(8) Gustafsson, K.; Andersson, S. Infrared Spectroscopy of Physisorbed and Chemisorbed $O_2$ on Pt(111). *J. Chem. Phys.* **2004**, *120*, 7750–7754.

(9) Beckerle, J. D.; Yang, Q. Y.; Johnson, A. D.; Ceyer, S. T. The Adsorption of CO and $O_2$ on Ni(111) at 8 K. *Surf. Sci.* **1988**, *195*, 77–93.

(10) Eichler, A.; Mittendorfer, F.; Hafner J. Precursor-Mediated Adsorption of Oxygen on the (111) Surfaces of Platinum-Group Metals. *J. Phys. Rev. B* **2000**, *62*, 4744–4755.

(11) Lahr, D. L.; Ceyer, S. T. Catalyzed CO Oxidation at 70 K on an Extended Au/Ni Surface Alloy. *J. Am. Chem. Soc.* **2006**, *128*, 1800–1801.

(12) Lahr, D. L. Molecular Oxygen Adsorbates at a Au/Ni(111) Surface Alloy and Their Role in Catalytic CO Oxidation at 70–250 K. Ph.D. Dissertation [Online], Massachusetts Institute of Technology, Cambridge, MA, June 2006. http://hdl.handle.net/1721.1/36250 (accessed Oct 25, 2013).

(13) Umezawa, K.; Nakanishi, S.; Gibson, W. M. Growth Modes Depending on the Growing Temperature in Heteroepitaxy: Au/Ni(111). *Phys. Rev. B.* **1998**, *57*, 8842–8844.

(14) Zafeiratos, S.; Kennou, S. Photoelectron Spectroscopy Study of Surface Alloying in the Au/Ni (s) [5(001)×(111)] System. *Appl. Surf. Sci.* **2001**, *173*, 69–75.

(15) Vattuone, L.; Gambardella, P.; Valbusa, U.; Rocca, M. HREELS Study of $O_2$ Molecular Chemisorption on Ag(001) *Surf. Sci.*, **1997**, *377–379*, 671–675.

(16) Sexton, B. A.; Madix, R. J. Vibrational Spectra of Molecular and Atomic Oxygen on Ag(110) *Chem. Phys. Lett.*, **1980**, *76*, 294–297.

(17) Prabhakaran, K.; Rao, C. N. R. A Combined EELS-XPS Study of Molecularly Chemisorbed Oxygen on Silver Surfaces: Evidence for Superoxo and Peroxo Species *Surf. Sci. Lett.*, **1987**, *186*, L575–L580.

(18) Hammer, B.; Nørskov, J. K. Theory of Adsorption and Surface Reactions. In *Chemisorption and Reactivity on Supported Clusters and Thin Films*; Lambert, R. M., Pacchioni, G., Eds.; Kluwer Academic: Dordrecht, Netherlands, 1997, pp 285–351.

(19) Nielsen, L. P. The Nucleation and Growth of Au on Ni(110) and Ni(111) – A Scanning Tunneling Microscopy Study. Ph.D. Dissertation [Online], Aarhus University, DK-8000 Aarhus C, Denmark, November 1995. http://phys.au.dk/fileadmin/site_files/publikationer/phd/Lars_Pleth_Nielsen.pdf (accessed Oct 25, 2013).

(20) Umezawa, K.; Nakanishi, S.; Gibson, W. M. Surface Structure and Metal Epitaxy: Impact Collision Ion Scattering Spectroscopy Studies on Au–Ni(111). *Surf. Sci.* **1999**, *426*, 225–234.

(21) Jacobsen, J.; Nielsen, L. P.; Besenbacher, F.; Stensgaard, I.; Lægsgaard, E.; Rasmussen, T.; Jacobsen K. W.; Nørskov, J. K. Atomic-Scale Determination of Misfit Dislocation Loops at Metal-Metal Interfaces. *Phys. Rev. Lett.* **1995**, *75*, 489–492.

(22) Ceyer, S. T.; Gladstone, D. J.; McGonigal, M.; Schulberg, M. T. Molecular Beams: Probes of the Dynamics of Reactions on Surfaces. In *Physical Methods of Chemistry*, 2nd ed.; Rossiter, B. W., Baetzold, R. C., Eds.; Wiley: New York, 1993, Vol. IXA; pp 383–452.

(23) Fischer, J. D. The Adsorption of Molecular Oxygen on Au/Ni(111) Alloys and its Oxidation of CO at 85 K. Ph.D. Dissertation [Online], Massachusetts Institute of Technology, Cambridge, MA, August 2010. http://hdl.handle.net/1721.1/62054 (accessed Oct 25, 2013).

(24) Tang, S. L. Dynamics of Chemisorption: CO on Ni(111). Ph.D. Dissertation [Online], Massachusetts Institute of Technology, Cambridge, MA, September 1985. http://hdl.handle.net/1721.1/15289 (accessed Oct 25, 2013).

(25) Outka, D. A.; Stöhr, J.; Jark, W.; Stevens, P.; Solomon, J.; Madix, R. J. Orientation and

Bond Length of Molecular Oxygen on Ag(110) and Pt(111): A Near-Edge X-Ray-Absorption Fine-Structure Study. *Phys. Rev. B*, **1987**, *35*, 4119–4122.

(26) Ibach, H. Vibrational Excitations at Surfaces. In *Physics of Surfaces and Interfaces* [Online]; Springer: Berlin, Germany, 2006; Chapter 7, pp 309–377. http://dx.doi.org/10.1007/3-540-34710-0_7 (accessed May 12, 2014).

(27) Childs, K. D.; Carlson, B. A.; LaVanier, L. A.; Moulder, J. F.; Paul, D. F.; Stickle, W. F.; Watson, D. G. *Handbook of Auger Electron Spectroscopy*, 3rd ed.; Physical Electronics, Inc.: Eden Prairie, MN, 1996.

(28) Baker, B. G.; Johnson, B. B.; Maire, G. L. C. Photoelectric Work Function Measurements on Nickel Crystals and Films. *Surf. Sci.* **1971**, *24*, 572–586.

(29) Holmblad, P. M.; Larsen J. H.; Chorkendorff, I. Modification of Ni(111) Reactivity Toward $CH_4$, CO, and $D_2$ by Two Dimensional Alloying. *J. Chem. Phys*. **1996**, *104*, 7289–7295.

(30) Kelley, M. J.; Gilmour, P. W.; Swartzfager, D. G. Strain Effects in Surface Segregation-The Au/Ni System. *J. Vac. Sci. Technol.* **1980**, *17*, 634–637.

(31) Caputi, L. S.; Jiang, S. L.; Amoddeo, A.; Tucci, R. Oxygen-Nickel Bond Length in Ni(111)-*p*(2×2)O Determined by Electron-Energy-Loss Fine-Structure Spectroscopy. *Phys. Rev. B* **1990**, *41*, 8513–8515.

(32) Marcus, P. M.; Demuth, J. E.; Jepsen, D. W. Determination of the Structure of Ordered Adsorbed Layers by Analysis of LEED Spectra. *Surf. Sci.* **1975**, *53*, 501–522.

(33) Menezes, W.; Knipp, P.; Tisdale, G.; Sibener, S. J. Surface Phonon Spectroscopy of Ni(111) Studied by Inelastic Electron Scattering. *Phys. Rev. B* **1990**, *41*, 5648–5651.

(34) Rybkin, A. G.; Usachev, D. Yu.; Varykhalov, A. Yu.; Shikin, A. M.; Adamchuk, V. K. Electronic Structure of Gold Nanoclusters on Oxidized Ni(755) Surface. *Phys. Solid State,* **2007**, *49*, 984–990. Original Russian text published in Fizika Tverdogo Tela, **2007**, *49*, 933–939.

(35) Besenbacher, F.; Nielsen, L. P.; Sprunger, P. T. Surface Alloying in Heteroepitaxial Metal-On-Metal Growth. In *The Chemical Physics of Solid Surfaces: Growth and Properties of Ultrathin Epitaxial Layers*; King, D. A., Woodruff, D. P., Eds.; Elsevier: Amsterdam, Netherlands, 1997; pp 207–257.

(36) Zion, B. D.; Hanbicki, A. T.; Sibener, S. J. Kinetic Energy Effects on the Oxidation of Ni(111) Using $O_2$ Molecular Beams. *Surf. Sci.* **1998**, *417*, L154–L159.

(37) Shrager, R. I. Nonlinear Regression With Linear Constraints: An Extension of the Magnified Diagonal Method. *J. Assoc. Comput. Mach.* **1970**, *17*, 446–452.

(38) Pireaux, J. J.; Liehr, M.; Thiry, P. A.; Delrue, J. P.; Caudano, R. Electron Spectroscopic Characterization of Oxygen Adsorption on Gold Surfaces: II. Production of Gold Oxide in Oxygen DC Reactive Sputtering. *Surf. Sci.* **1984**, *141*, 221–232.

(39) Parker, D. H.; Bartram, M. E.; Koel, B. E. Study of High Coverages of Atomic Oxygen on the Pt(111) Surface. *Surf. Sci.* **1989**, *217*, 489–510.

(40) Nørskov, J. K.; Rossmeisl, J.; Logadottir, A.; Lindqvist, L.; Kitchin, J. R.; Bligaard, T.; Jónsson, H. Origin of the Overpotential for Oxygen Reduction at a Fuel-Cell Cathode. *J. Phys. Chem. B* **2004**, *108*, 17886–17892.

(41) Nørskov, J. K.; Bligaard, T.; Logadottir, A.; Bahn, S.; Hansen, L. B.; Bollinger, M.; Bengaard, H.; Hammer, B.; Sljivancanin, Z.; Mavrikakis, M.; Xu, Y.; Dahl, S.; Jacobsen, C.

J. H. Universality in Heterogeneous Catalysis. *J. Catal.* **2002**, *209*, 275–278.

(42) Saliba, N.; Parker, D. H.; Koel, B. E. Adsorption of Oxygen on Au(111) by Exposure to Ozone. *Surf. Sci.* **1998**, *410*, 270–282.

(43) Hammer, B.; Nørskov, J. K. Theoretical Surface Science and Catalysis – Calculations and Concepts. In *Advances in Catalysis*; Gates, B. C., Knozinger, H., Eds.; Academic Press: San Diego, California, 2000, vol. 45, pp 71–129.

(44) Hammer, B.; Nørskov, J. K. Electronic Factors Determining the Reactivity of Metal Surfaces. *Surf. Sci.*, **1995**, *343*, 211–220.

(45) Kitchin, J. R.; Nørskov, J. K.; Barteau, M. A.; Chen, J. G. Role of Strain and Ligand Effects in the Modification of the Electronic and Chemical Properties of Bimetallic Surfaces. *Phys. Rev. Lett.* **2004***, 93*, 156801.

(46) Hammer, B; Nørskov, J. K. Why Gold is the Noblest of All the Metals. *Nat.* **1995**, *376*, 238–240.

(47) Ruban, A.; Hammer, B.; Stoltze, P.; Skriver, H. L.; Nørskov, J. K. Surface Electronic Structure and Reactivity of Transition and Noble Metals. *J. Mol. Catal. A* **1997**, *115*, 421–429.

(48) García-Mota, M.; López, N. The Role of Long-Lived Oxygen Precursors on AuM Alloys (M = Ni, Pd, Pt) in CO Oxidation. *Phys. Chem. Chem. Phys.* **2011**, *13*, 5790–5797.